analytical chemistry

pubs.acs.org/ac Article

DNA-Mediated Au−Au Dimer-Based Surface Plasmon Coupling Electrochemiluminescence Sensor for BRCA1 Gene Detection

Qian Zhang, Yu Tian, Zihui Liang, Zizhun Wang, Shuping Xu, and Qiang Ma*

Cite This: *Anal. Chem.* 2021, 93, 3308−3314 Read Online

ACCESS | Metrics & More | Article Recommendations | Supporting Information

ABSTRACT: Herein, we constructed a DNA-mediated Au−Au dimer-based surface plasmon coupling electrochemiluminescence (SPC-ECL) sensor. In the SPC-ECL sensing system, graphite phase carbon nitride quantum dots (GCN QDs) worked as an ECL emitter. A DNA rigid chain structure was employed to connect two Au NPs in an equilateral triangle configuration to form the Au−Au dimers. Due to the hot spot effect, the designed Au−Au dimers had a strong electromagnetic field intensity, which can greatly enhance the ECL signal of GCN QDs than a single Au nanoparticle. The gap distance of dimers can be effectively regulated by the DNA length, which resulted in different electromagnetic field intensities. Therefore, the different SPC-ECL amplification effects on the GCN QD signal by Au−Au dimers have been revealed. The maximum ECL signal of GCN QDs can be enhanced fourfold based on the Au−Au dimers with a gap distance of 2 nm. Furthermore, the biosensor showed good analytical performance for the detection of breast cancer susceptibility gene 1 (BRCA1 genes) (1 fM−1 nM) with a detection limit of 0.83 fM. This work provided an effective and precise SPC-ECL sensing mode for the diagnosis and prognosis of breast cancer.

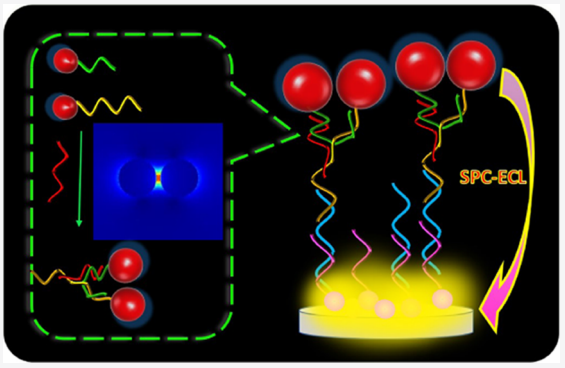

INTRODUCTION

According to World Health Organization (WHO) statistics, breast cancer has the highest female morbidity and mortality of cancer types in the world. In 2018, the number of new cases of breast cancer reached 2.088 million, accounting for 11.6% of new cases.[1] More notably, triple-negative breast cancer (TNBC) accounts for 15% of the incidence of breast cancer.[2] TNBC is highly concealed and hard to be diagnosed, which only is treated by clinical surgery or chemotherapy. Therefore, early diagnosis is very important for TNBC detection. Breast cancer susceptibility gene 1 (BRCA1 gene) is the most important tumor suppressor gene related to the occurrence and development of breast cancer, especially TNBC.[3] People with BRCA1 gene mutations have a much higher risk of breast cancer than those without mutations. BRCA1 gene mutations exist in 1/3 of TNBC patients.[4,5] At present, the method of gene detection is still based on clinical technology, which is time-consuming and expensive. Thus, it is necessary to establish a sensitive and rapid method for the detection of the BRCA1 gene.

Electrochemiluminescence is an analytical technique with a low detection limit, high detection speed, and high accuracy. Surface-enhanced ECL is an important sensing mode and strongly dependent on the localized surface plasmon resonance (LSPR) of plasmonic materials.[6,7] Xu's group first reported the impact of the LSPR effect on the ECL signal.[8] We have further studied the important factors of surface-enhanced ECL, including wavelength-dependence, the distance between QDs and plasmonic material, and the plasmonic material structure.[9−12] The LSPR of plasmonic materials is closely related to the ECL enhancement amplitude, which can further improve the signal intensity and the sensitivity of the ECL detection. Until now, most widely used plasmonic materials in the surface-enhanced ECL sensor are noble metal monomers, such as gold nanoparticles (Au NP),[10] gold nanodendrites,[13,14] and gold nanotubes.[15] However, the LSPR effect of metal monomers is not satisfactory for ECL enhancement. Therefore, it is necessary and meaningful to explore plasmonic materials with a stronger LSPR effect. Plasmonic dimers have attracted considerable attention due to their enlarged electric field.[16−18] At the junction of two NPs, surface plasmon coupling (SPC) between two NPs can result in a high electromagnetic field enhancement (hot spot effect).[19−21] This SPC-induced ECL sensing is named surface plasmon coupling electrochemiluminescence (SPC-ECL). The SPC-ECL sensing mode provided a high sensitive sensing mode, which was first reported in 2018.[22] However, there are still some issues in the initial SPC-ECL research. For example, the gap distance effect

Received: December 28, 2020
Accepted: January 22, 2021
Published: February 3, 2021

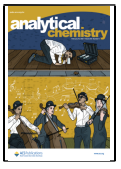

https://dx.doi.org/10.1021/acs.analchem.0c05440
Anal. Chem. 2021, 93, 3308−3314

Scheme 1. Schematic Illustration of the ECL Sensor

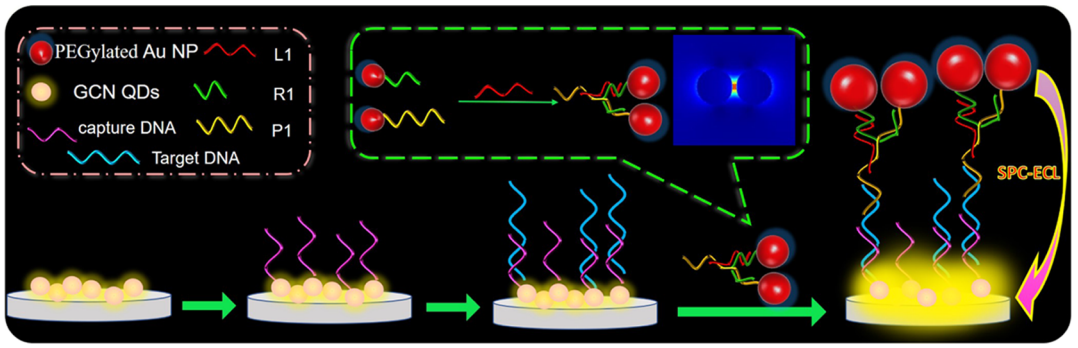

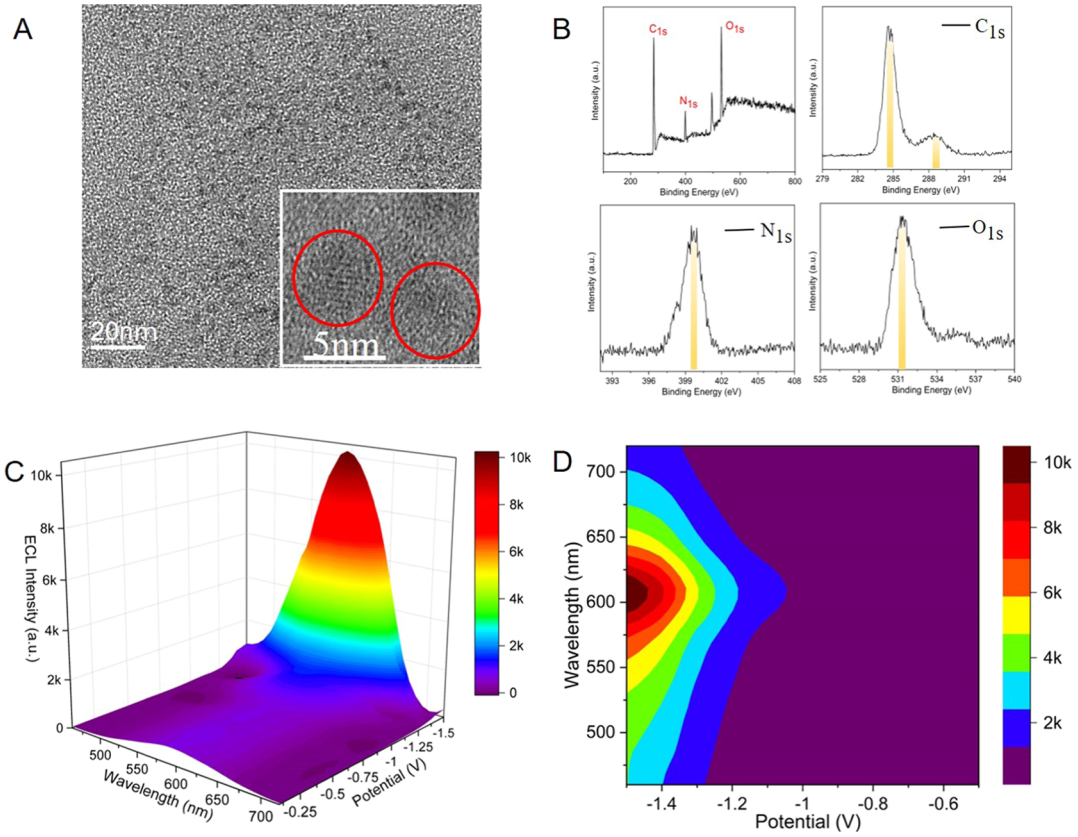

Figure 1. (A) TEM image of GCN QDs. The inset of (A) corresponds to the enlarged image with the scale bar of 5 nm. (B) XPS spectra of GCN QDs. (C) The three-dimensional ECL spectrum and (D) the heat map image of GCN QDs in PBS containing 10 mM $K_2S_2O_8$.

of the dimers on the ECL signal is not clear. The regulation and application of the hot spot effect on the ECL sensor need to be further explored.

In this work, we assembled the Au−Au dimers through a DNA rigid chain structure to construct a biosensor (Scheme 1). A DNA molecule is an excellent template, which can combine two separate plasmons into a specific shape of a DNA-mediated dimer.[23,24] First, Au NPs were asymmetrically modified with mPEG-SH and connected to thiolated DNA. Then, the complementation between DNA bases was used to assemble two Au NPs into an Au−Au dimer in the form of triangles. The DNA chain can not only regulate the distance of the dimer but also keep the binding site for biosensing. Furthermore, we prepared the Au−Au dimers with different gap distances via the different DNA lengths. The relation of the Au−Au dimers with different gap distances on the electromagnetic field intensity and ECL enhancement was discussed. Finally, we constructed a sandwich sensor with the SPC-ECL mode to detect the BRCA1 gene, which exhibited great potential for clinical diagnosis.

EXPERIMENTAL SECTION

Synthesis of Au−Au Dimers. Au nanoparticles of about 19 nm were prepared by citric acid reduction. According to the literature,[25] Au NPs were asymmetrically modified with mPEG-SH. Then, the asymmetrically PEGylated AuNPs were attached to two groups of thiolated DNA. In brief, 100 μL of 1 μM thiolated DNA (R1 or P1) was mixed with 500 μL of asymmetrically modified AuNPs. Then, 10 μL of 0.1 M NaCl was added into the above solution and aged for 24 h under slow shaking. In the next step, NPs were resuspended in 500 μL of Tris−HCl buffer after centrifugation to obtain the

https://dx.doi.org/10.1021/acs.analchem.0c05440
Anal. Chem. 2021, 93, 3308−3314

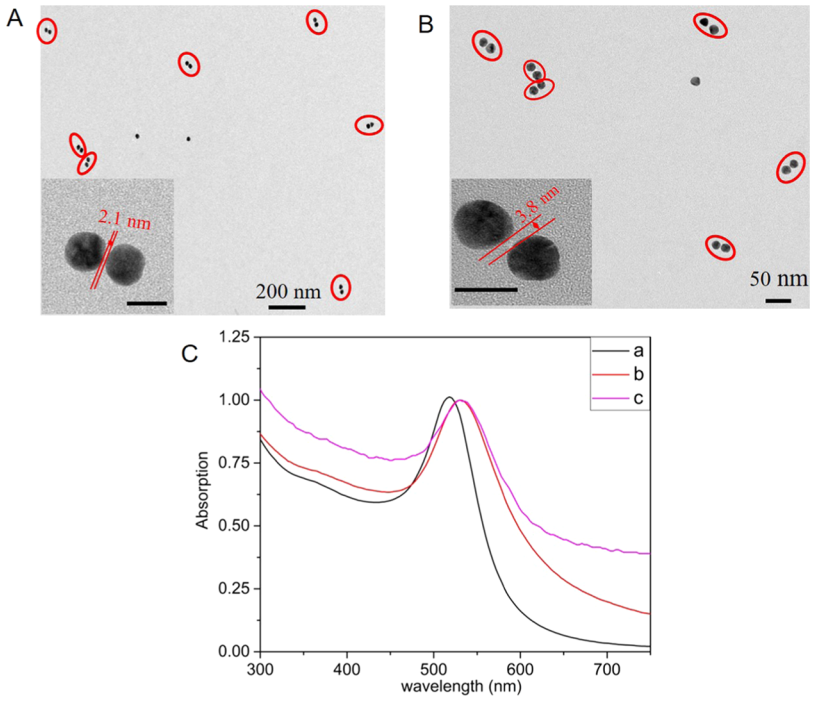

Figure 2. TEM image (A) of Au−Au-1 dimers and (B) Au−Au-3 dimers. The insets of (A) and (B) correspond to the enlarged image with the scale bar of 20 nm. (C) The UV−vis absorption spectra of Au NPs (a), the asymmetrically PEGylated Au NPs (b), and Au−Au dimers (c).

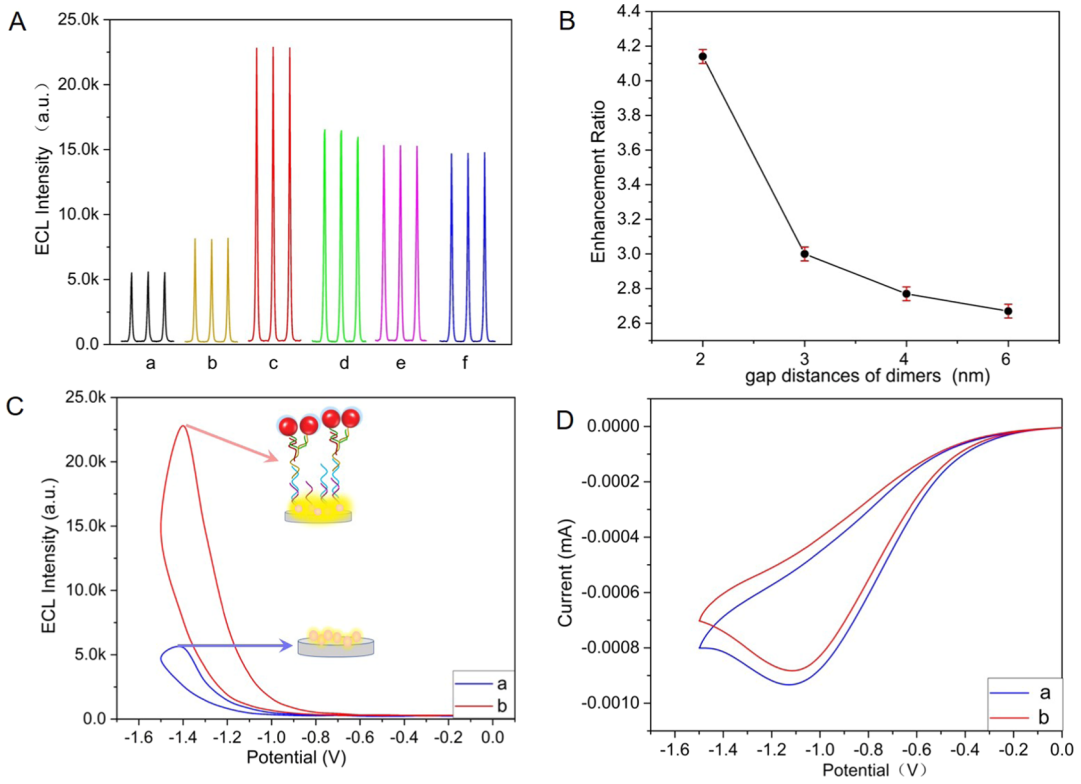

Figure 3. (A) ECL responses of (a) GCN QDs, (b) GCN QDs with Au NPs, (c) GCN QDs with Au−Au-1 dimers, (d) GCN QDs with Au−Au-2 dimers, (e) GCN QDs with Au−Au-3 dimers, and (f) GCN QDs with Au−Au-4 dimers in 0.1 M pH 7.4 PBS containing 0.1 M $K_2S_2O_8$. (B) The enhancement ratio of GCN QDs with Au−Au dimers of different gap distances. (C) ECL-potential curves and (D) cyclic voltammograms (CV) of GCN QDs (a) and GCN QDs with Au−Au-1 dimers (b).

asymmetrically modified Au-R1 or Au-P1. At last, each 150 μL of Au-R1, Au-P1, and L1 was hybridized at 37 °C for 1 h. Au−Au dimers with other gap distances were prepared by the above procedure using the corresponding DNA in place of P1, R1, and L1. The formed Au−Au dimers were preserved at 4 °C. The four dimers with different distances were named Au−Au-1 dimers, Au−Au-2 dimers, Au−Au-3 dimers, and Au−Au-4 dimers according to the length of DNA.

https://dx.doi.org/10.1021/acs.analchem.0c05440
Anal. Chem. 2021, 93, 3308−3314

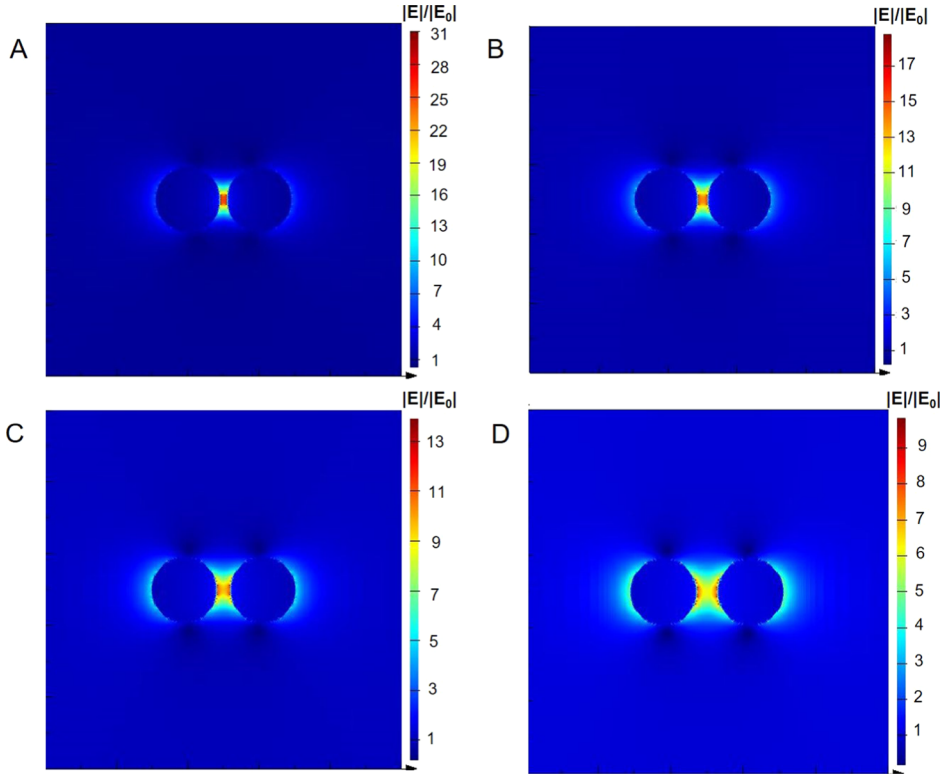

Figure 4. FDTD simulation of electromagnetic field intensity distributions of Au−Au dimers with different gap distances of (A) 2 nm, (B) 3 nm, (C) 4 nm, and (D) 6 nm.

SPC-ECL Sensor Construction and the Analytical Procedure. First, 6 μL of graphite phase carbon nitride quantum dots (GCN QDs)/capture DNA was dropped on a pretreated glassy carbon electrode (GCE) to form capture DNA/GCNQDs/GCE. Next, bovine serum albumin was used to block the nonspecific sites. Then, the target DNA with different concentrations was hybridized to capture DNA at 37 °C for 1 h. After that, Au−Au dimers were attached to the surface of the GCE by hybridization with the target DNA. The ECL measurements were accomplished in 0.1 M pH 7.4 $K_2S_2O_8$/phosphate buffer saline (PBS). The voltage of the photomultiplier tube was 800 V. The scanning potential ranged from −1.5 to 0 V.

Simulation of Hot Spot Distribution by Finite-Difference Time Domain (FDTD). The FDTD method was completed by Commercial Software (Lumerical Solutions, Inc.) to simulate the electromagnetic field distribution around Au−Au dimers. In the simulations, the models of Au NPs were set as spheres and the size of Au NPs was 19 nm. The refractive index of the surrounding medium was 1.33 and the wavelength of the incident light was set at 608 nm.

RESULTS AND DISCUSSION

Characterization of GCN QDs and Au−Au Dimers. The transmission electron microscopy (TEM) image (Figure 1A) shows that the average diameter of GCN QDs is 4 nm. X-ray photoelectron spectroscopy (XPS) data of GCN QDs are recorded in Figure 1B. The peaks at 284.6 eV (C_{1s}), 399.6 eV (N_{1s}), and 531.4 eV (O_{1s}) are detected, which indicates that the GCN QDs are successfully prepared. The three-dimensional ECL spectrum of GCN QDs is displayed in Figure 1C,D. Obviously, when the potential is −1.5 V and the wavelength is 608 nm, the color graph is the brightest, which means that GCN QDs have the strongest ECL signal.

The morphology of Au−Au dimers is characterized by TEM. In Figure 2, the average diameter of Au NPs is 19 nm. Figure 2A shows that Au−Au dimers have good dispersion and high yield (about 70%). It is attributed to the asymmetric modification of Au NPs and the special DNA configuration. As exhibited in the enlarged image of Figure 2A,B, the interparticle distances of Au−Au-1 and Au−Au-3 dimers are 2.1 and 3.8 nm, respectively. It is consistent with the length (2, 4 nm) calculated from the corresponding DNA (R1, R3). Therefore, it is calculated that the gap distances of Au−Au-2 and Au−Au-4 dimers are 3 and 6 nm, respectively. Figure 2C shows the UV−vis absorption spectrum of Au NPs (a), the asymmetrically PEGylated Au NPs (b), and Au−Au dimers (c). The absorption peak of Au NPs can be observed at 518 nm. The absorption peaks of the PEGylated Au NPs (b) and Au−Au dimers (c) shift to 527 nm.

ECL Enhancement Mechanism of Au−Au Dimers. Figure 3A shows the enhancement effect of Au NPs and different Au−Au dimers on the ECL signal of GCN QDs. Although Au NPs and Au−Au dimers can enhance the ECL signal, the enhancement extent is quite different. The original ECL signal of GCN QDs is ca. 5.5k (curve a). The ECL signal of GCN QDs shows 1.5-fold enhancement with Au NPs. The ECL signal of GCN QDs increases with the SPR effect of Au NPs (curve b, ca. 8.0k). When Au−Au-1 dimers are modified on GCE, the ECL signal of GCN QDs is greatly improved (curve c, ca. 22.8k). When Au−Au-2 dimers, Au−Au-3 dimers, and Au−Au-4 dimers are added, respectively, the corresponding ECL signals of GCN QDs are 16.5k (curve d), 15.3k (curve e), and 14.7k (curve f). The enhancement ratio of Au−Au dimers with different gap distances in the ECL signal of

https://dx.doi.org/10.1021/acs.analchem.0c05440
Anal. Chem. 2021, 93, 3308−3314

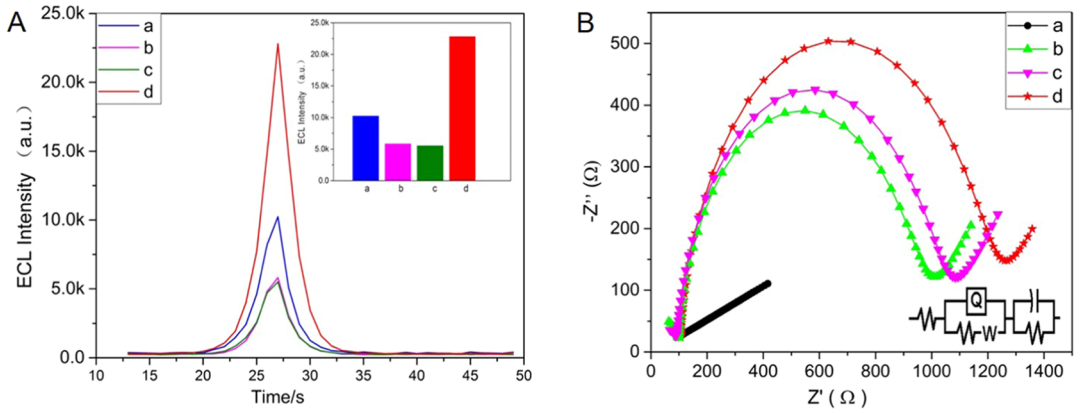

Figure 5. (A) ECL responses of the modified electrode step by step: (a) GCN QDs/GCE, (b) capture DNA/GCN QDs/GCE, (c) target DNA/capture DNA/GCN QDs/GCE, and (d) Au−Au dimers/target DNA/capture DNA/GCN QDs/GCE. The inset bar graph depicts the ECL responses of the modified electrode from a to d. (B) EIS of (a) GCE, (b) captured DNA/GCN QDs/GCE, (c) target DNA/GCN QDs/GCE, and (d) Au−Au dimers/target DNA/capture DNA/GCN QDs/GCE in a 2.5 mM $[Fe(CN)_6]^{3^-/4^-}$ solution containing 0.1 M KCl.

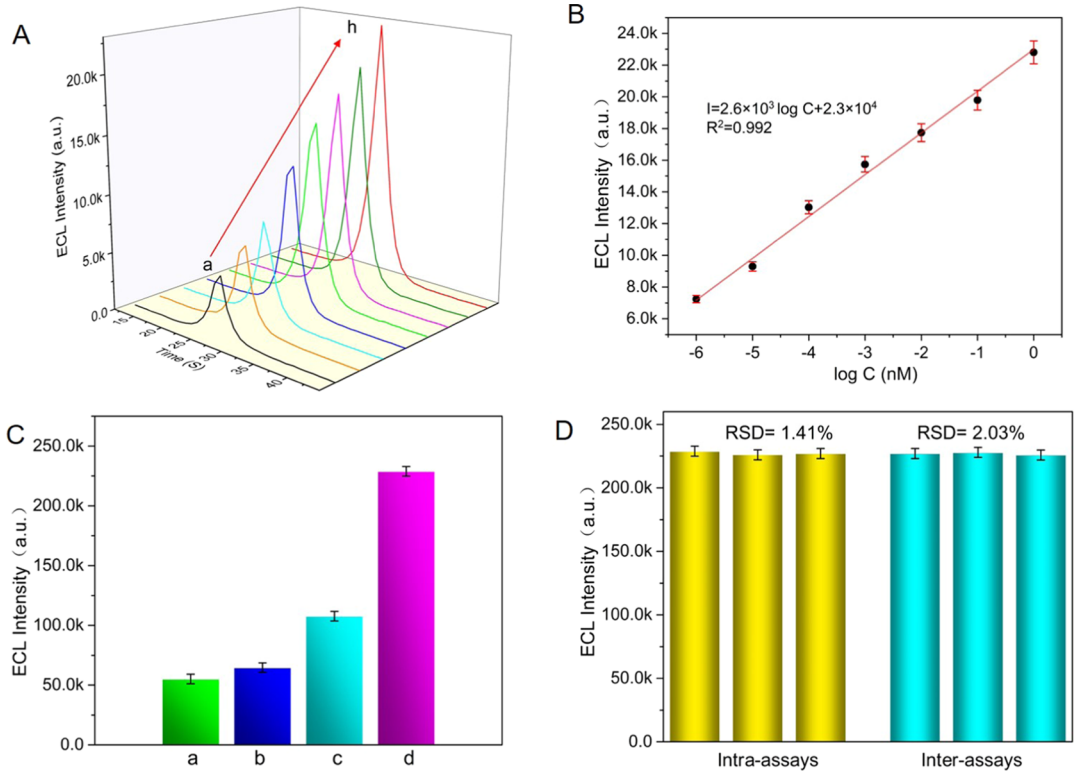

Figure 6. (A) Relationship between the ECL intensity and different BRAF gene concentrations (from a to h): blank, 10^{-6}, 10^{-5}, 10^{-4}, 10^{-3}, 10^{-2}, 10^{-1}, and 1 nM. (B) The corresponding linear relationship for BRCA1 gene detection. (C) Selectivity of the sensing strategy: (a) blank, (b) triple-MT, (c) one-MT, and (d) complementary target DNA. The concentration of DNA is 1 nM. (D) The repeatability of the sensor was investigated by intra- and interassays.

GCN QDs are recorded in Figure 3B. There are 4.1-, 3.0-, 2.8-, 2.7-fold enhancement on the GCN QD ECL signals based on the Au−Au dimers of 2, 3, 4, and 6 nm, respectively. The Au−Au dimer-induced ECL signal enhancement ratio far exceeds that induced by Au NPs. The strong electromagnetic field is distributed around the dimer, which can accelerate the excitation rate of QDs and induce ECL signal enhancement.[13] Especially in the adjacency of the Au−Au dimers, the surface plasmons of Au NPs are coupled with each other. It results in an enhancement of the electromagnetic field (hot spot effect), hence enhancing the ECL signal. When the distance between the two Au NPs is relatively closer, the hot spot effect is more significant. So, the ECL enhancement amplitude is higher. SPC-ECL can be understood as the process of the ECL signal enhancement generated by electromagnetic field stimulation. For the Au−Au dimers/GCN QDs/$K_2S_2O_8$ system in this article, the ECL mechanism is as follows.

$$\text{GCN QD} + e^- \rightarrow \text{GCN QD}^{\bullet -} \quad (1)$$

$$S_2O_8^{2-} + e^- \rightarrow SO_4^{2-} + SO_4^{\bullet -} \quad (2)$$

https://dx.doi.org/10.1021/acs.analchem.0c05440
Anal. Chem. 2021, 93, 3308−3314

$$\text{GCN QD}^{\bullet -} + \text{SO}_4^{\bullet -} \xrightarrow{\text{Au–Au dimers}} \text{GCN QD}^{*} + \text{SO}_4^{2-} \quad (3)$$

$$\text{GCN QD}^{*} \rightarrow \text{GCN Qs} + h\nu \quad (4)$$

GCN QD obtains electrons and becomes an anion radical ($GCN\ QD^{\bullet -}$). Then, $GCN\ QD^{\bullet -}$ reacts with sulfuric acid radicals ($SO_4^{\bullet -}$) generated by sulfate radicals to generate an excited state (GCN QD*). Next, GCN QD* returns to the ground state and emits orange light. In the presence of Au−Au dimers, the apparent increase in the ECL signal intensity is mainly due to changes in the process of excited-state generation.

To further illustrate the ECL enhancement mechanism, FDTD is used to simulate the electromagnetic field distribution on Au−Au dimers with different gap distances. As depicted in Figure 4, there are obvious differences in the electromagnetic field intensity of Au−Au dimers with different gap distances. The electromagnetic field distribution of Au−Au dimers has obvious regionality. The plasmon coupling of the adjacent of the dimer produces a higher electromagnetic field intensity than the side. From Figures 4A−D, it can be found that the electromagnetic field intensity is gradually weakened with the increase of the gap distances of the dimer (from 2 to 6 nm). In particular, the electromagnetic field intensity adjacent to NPs drops 3.4-fold. As a result, the ECL enhancement ratio with Au−Au dimers decreases.

To verify the reaction mechanism, ECL-potential curves and cyclic voltammograms (CV) are investigated. In Figure 3C, when the Au−Au-1 dimer is introduced into the electrode surface (curve a), the ECL response of GCN QDs shows 4-fold enhancement. Figure 3D depicts that the reduction peak of GCN QDs is −1.1 V (curve a). The reduction peak of GCN QDs with Au−Au-1 dimers (curve b) shifts to −0.9 V. It indicates that the ECL reaction becomes more effective with the assistance of Au−Au dimers. It is because Au−Au dimers can generate a strong electromagnetic field to accelerate the excitation rate of QDs.[13] Therefore, Au−Au dimers with a gap distance of 2 nm are selected as plasmonic materials to construct the SCP-ECL sensor.

Analytical Performance of the SPC-ECL Sensor. Figure 5A shows the ECL response of the sensor construction process. The ECL signal of GCN QDs is about 5.5k (curve a). After the modification of the capture DNA (curve b) and target DNA (curve c), the corresponding ECL signal decreases. It is caused because the electron transfer resistance on the electrode surface increases. When Au−Au dimers are assembled on the surface of the electrode (curve d), the ECL signal is significantly enhanced due to the strong electromagnetic field generated with the hot spot effect. The changes of the GCE surface state are recorded by electrochemical impedance spectroscopy (EIS). Figure 5B shows that the electron transfer resistance (Ret) of the pretreated GCE (curve a) is very small. The semicircle diameter of captured DNA/GCN QDs/GCE is increased clearly (curve b, Ret = 850.6 Ω). When the target DNA (curve c, Ret = 934.8 Ω) and Au−Au dimers (curve d, Ret = 1095 Ω) are modified on the surface of GCE, the Ret increases gradually due to the nonconductivity of DNA. The above results indicate the ECL sensor is constructed successfully.

The analysis performance of the SPC-ECL sensor is validated by investigating the sensitivity, selectivity, and stability of the sensor. Figure 6A clearly shows that as the target DNA concentration is added, the ECL response gradually becomes stronger (1 fM−1 nM). Figure 6B depicts the linear relationship between the ECL intensity (I) and the logarithm of the BRCA1 gene concentration (lg C). The detection limit of this sensor is calculated to be 0.83 fM (S/N = 3). Table S2 records the comparison of the detection performance of the SPC-ECL sensor and other reports for the determination of the BRCA1 gene. Moreover, the ECL response to interferences including one-MT and triple-MT can evaluate the selectivity of the biosensor. As shown in Figure 6C, the ECL signal of the complementary target DNA is much higher than that of one-MT and triple-MT. The results demonstrate that the biosensor has a good selectivity. Furthermore, the stability of the sensor is investigated and recorded in Figure 6D. The ECL sensor showed good stability in both intra- (relative standard deviation (RSD) ≤ 1.4%) and interassays (RSD ≤ 2.0%). The analytical performance of the sensor in actual samples is investigated by standard addition methods. It can be seen from Table 1 that the recoveries of human serum are in the range of 91.0−108% (RSD ≤ 4.86%). The SPC-ECL sensor has perfect potential application in clinical detection.

Table 1. Determination of Target DNA in Serum Samples

sample	spiked (nM)	founded (nM)	recovery (%)	RSD (%) (n = 3)
1	1.0	1.08	108.0	3.03
2	0.01	0.0091	91.0	2.17
3	0.001	0.00101	101.0	4.86

CONCLUSIONS

In this paper, we constructed an SPC-ECL sensor based on DNA-mediated Au−Au dimers to detect the BRCA1 gene. A DNA molecule is used to assemble two Au NPs into Au−Au dimers. Meanwhile, it precisely regulates the gap distances of the Au−Au dimers. Furthermore, we have discussed the hot spot effect of Au−Au dimers on the ECL signal. The Au−Au dimers with a gap distance of 2 nm have the strongest hot spot to enhance the ECL signal of GCN QDs. Based on the hot spot effect of Au−Au dimers, the SPC-ECL sensor shows good sensitivity and specificity for detecting the BRCA1 gene. There are still some unresolved issues in the SPC-ECL research. To improve the valuable performance of SPC-ECL, the local morphology of the plasmonic dimer still needs to be studied further in the future.

ASSOCIATED CONTENT

Supporting Information

The Supporting Information is available free of charge at https://pubs.acs.org/doi/10.1021/acs.analchem.0c05440.

Chemicals and the apparatus, syntheses of GCN QDs and the GCN QD/capture DNA conjugate, serum sample testing, the DNA sequences in present work (Table S1), and the comparison of the various methods for detecting the BRCA1 gene (Table S2) (PDF)

AUTHOR INFORMATION

Corresponding Author

Qiang Ma − *Department of Analytical Chemistry, College of Chemistry, Jilin University, Changchun 130012, China;*

https://dx.doi.org/10.1021/acs.analchem.0c05440
Anal. Chem. 2021, 93, 3308−3314

orcid.org/0000-0003-4841-5005; Phone: : +86-431-85168352; Email: qma@jlu.edu.cn

Authors

Qian Zhang − *Department of Analytical Chemistry, College of Chemistry, Jilin University, Changchun 130012, China*

Yu Tian − *State Key Laboratory of Supramolecular Structure and Materials, Institute of Theoretical Chemistry, College of Chemistry, Jilin University, Changchun 130012, China*

Zihui Liang − *Department of Analytical Chemistry, College of Chemistry, Jilin University, Changchun 130012, China*

Zizhun Wang − *Electron Microscopy Center, Jilin University, Changchun 130012, China*

Shuping Xu − *State Key Laboratory of Supramolecular Structure and Materials, Institute of Theoretical Chemistry, College of Chemistry, Jilin University, Changchun 130012, China;* orcid.org/0000-0002-6216-6175

Complete contact information is available at: https://pubs.acs.org/10.1021/acs.analchem.0c05440

Author Contributions

Q.Z.: conceptualization, data curation, formal analysis, investigation, writing—original draft, and writing—review and editing; Y.T.: software; Z.L.: investigation; Z.W.: methodology; S.X.: software; and Q.M.: supervision, project administration, resources, and writing—review and editing.

Notes

The authors declare no competing financial interest.

The use of human serum samples in this work has been approved by the ethics committee of the Third Hospital of Jilin University (No. 2019-NSFC-051).

■ ACKNOWLEDGMENTS

The present work was supported by the Youth Science Fund of Jilin Province (20140520081JH) and the "Thirteenth Five Year" Project of the Science and Technology Research in the Education Department of Jilin Province, China.

■ REFERENCES

(1) Bray, F.; Ferlay, J.; Soerjomataram, I.; Siegel, R. L.; Torre, L. A.; Jemal, A. *Ca-Cancer J. Clin.* **2018**, *68*, 394−424.

(2) Denkert, C.; Liedtke, C.; Tutt, A.; von Minckwitz, G. *Lancet* **2017**, *389*, 2430−2442.

(3) Hall, J. M.; Lee, M. K.; Newman, B.; Morrow, J. E.; Anderson, L. A.; Huey, B.; King, M.-C. *Science* **1990**, *250*, 1684−1689.

(4) Bianchini, G.; Balko, J. M.; Mayer, I. A.; Sanders, M. E.; Gianni, L. *Nat. Rev. Clin. Oncol.* **2016**, *13*, 674−690.

(5) Shimelis, H.; LaDuca, H.; Hu, C.; Hart, S. N.; Na, J.; Thomas, A.; Akinhanmi, M.; Moore, R. M.; Brauch, H.; Cox, A.; Eccles, D. M.; Ewart-Toland, A.; Fasching, P. A.; Fostira, F.; Garber, J.; Godwin, A. K.; Konstantopoulou, I.; Nevanlinna, H.; Sharma, P.; Yannoukakos, D.; Yao, S.; Feng, B. J.; Tippin Davis, B.; Lilyquist, J.; Pesaran, T.; Goldgar, D. E.; Polley, E. C.; Dolinsky, J. S.; Couch, F. J. *J. Natl. Cancer Inst.* **2018**, *110*, 855−862.

(6) Wang, D.; Guo, L.; Huang, R.; Qiu, B.; Lin, Z.; Chen, G. *Electrochim. Acta* **2014**, *150*, 123−128.

(7) Lu, H. J.; Xu, C. H.; Xu, J. J.; Chen, H. Y. *Anal. Chem.* **2019**, *91*, 14757−14764.

(8) Shan, Y.; Xu, J. J.; Chen, H. Y. *Chem. Commun.* **2009**, 905−907.

(9) Wang, J.; Shan, Y.; Zhao, W. W.; Xu, J. J.; Chen, H. Y. *Anal. Chem.* **2011**, *83*, 4004−4011.

(10) Zhang, Q.; Liu, Y.; Nie, Y.; Liu, Y.; Ma, Q. *Anal. Chem.* **2019**, *91*, 13780−13786.

(11) Liu, Y.; Nie, Y.; Wang, M.; Zhang, Q.; Ma, Q. *Biosens. Bioelectron.* **2020**, *148*, No. 111823.

(12) Zhang, Q.; Liang, Z.; Nie, Y.; Zhang, X.; Ma, Q. *Mikrochim. Acta* **2020**, *187*, No. 599.

(13) Li, M. X.; Feng, Q. M.; Zhou, Z.; Zhao, W.; Xu, J. J.; Chen, H. Y. *Anal. Chem.* **2018**, *90*, 1340−1347.

(14) Zhanga, A.; Guob, W.; Keb, H.; Zhangb, X.; Zhangb, H.; Huangb, C.; Yangc, D.; Jiab, N.; Cui, D. *Biosens. Bioelectron.* **2018**, *101*, 219−226.

(15) Wang, H.; Yuan, Y.; Zhuo, Y.; Chai, Y.; Yuan, R. *Anal. Chem.* **2016**, *88*, 2258−2265.

(16) Tavakkoli Yaraki, M.; Daqiqeh Rezaei, S.; Tan, Y. N. *Phys. Chem. Chem. Phys.* **2020**, *22*, 5673−5687.

(17) Xu, L.; Sun, M.; Ma, W.; Kuang, H.; Xu, C. *Mater. Today* **2016**, *19*, 595−606.

(18) Jung-Hwan, S.; Raza, S.; Jorik van de, G.; Ju-Hyung, K.; Li, Q.; Kik, P. G.; Brongersma, M. L. *Nat. Commun.* **2021**, *12*, No. 48.

(19) Xu, L.; Ma, W.; Wang, L.; Xu, C.; Kuang, H.; Kotov, N. A. *Chem. Soc. Rev.* **2013**, *42*, 3114−3126.

(20) Kessentini, S.; Barchiesi, D.; D'Andrea, C.; Toma, A.; Guillot, N.; Di Fabrizio, E.; Fazio, B.; Maragó, O. M.; Gucciardi, P. G.; Lamy de la Chapelle, M. *J. Phys. Chem. C* **2014**, *118*, 3209−3219.

(21) Huang, Y.; Chen, Y.; Wang, L.-L.; Ringe, E. *J. Mater. Chem. C* **2018**, *6*, 9607−9614.

(22) Li, M.-X.; Zhang, N.; Zhao, W.; Luo, X.-L.; Chen, H.-Y.; Xu, J.-J. *Electrochem. Commun.* **2018**, *94*, 36−40.

(23) Peng, T.; Li, X.; Li, K.; Nie, Z.; Tan, W. *ACS Appl. Mater. Interfaces* **2020**, *12*, 14741−14760.

(24) Li, N.; Shang, Y.; Han, Z.; Wang, T.; Wang, Z. G.; Ding, B. *ACS Appl. Mater. Interfaces* **2019**, *11*, 13835−13852.

(25) Li, X. L.; Zhang, Z. L.; Zhao, W.; Xia, X. H.; Xu, J. J.; Chen, H. Y. *Chem. Sci.* **2016**, *7*, 3256−3263.